Sensing and Bio-Sensing Research 10 (2016) 34–40

Contents lists available at ScienceDirect

Sensing and Bio-Sensing Research

journal homepage: www.elsevier.com/locate/sbsr

Ammonia sensor and antibacterial activities of green zinc oxide nanoparticles

S. Khaleel Basha [a], K. Vijaya Lakshmi [b], V. Sugantha Kumari [b,*]

[a] Department of Chemistry, C. Abdul Hakeem College, Melvisharam 632 509, India
[b] Department of Chemistry, Auxilium College, Vellore 632 006, India

ARTICLE INFO

Article history:
Received 3 April 2016
Received in revised form 12 August 2016
Accepted 30 August 2016

Keywords:
Alginate
Zinc oxide nanoparticles
Antibacterial activity
Ammonia sensor

ABSTRACT

Zinc oxide nanoparticles was synthesized by alginate (A) through a rapid and a facile step in the aqueous solution condition at room temperature. Fabrication of zinc oxide nanoparticles was characterized by ATR-FTIR, TEM and XRD. ATR-FTIR analysis confirmed that the A/ZnO NPs were encapsulated by the polymerized alginate. Their shape, structure and composition were assessed by SEM. TEM and XRD analysis indicated that the A/ZnO NPs give evidence of the crystalline nature of ZnO and hybrid NPs structure, which is suitable for ammonia gas sensor development. The controlled size of the A/ZnO NPs obtained using this innovative synthesis strategy minimizes the response time of 2–3 s to sense the ammonia gas significantly with a detection limit of 1 ppm were found at room temperature. The antibacterial tests revealed that the A/ZnO NPs exhibits a potent activity against gram positive and gram negative bacteria.

1. Introduction

In the fields of nanotechnology metal oxides nanostructures stand out as being among the most versatile nanomaterials because of their excellent high surface area to volume ratio, low toxicity, are environment-friendly, have chemical stability and biocompatibility. Among metal Zinc oxide nanoparticles (ZnO NPs) are of the most promising metal oxides due to their attractive physical and chemical properties. Recently, fabrication of nanosized semiconductors rapidly increasing in regards to their novel optical, chemical, photoelectrochemical and electronic properties which are different from that of bulk [1]. Among various semiconductor materials, zinc oxide nanomaterials have attracted huge attention in sensing areas due to its relatively large surface area to volume ratio, larger band gap (3.37 eV at room temperature), high exciton binding energy (60 meV) which makes excitons in ZnO stable up to 350 K, high transparency, its high ionicity and biocompatibility [2]. ZnO NPs are the forefront of research due to their unique properties such as semiconductor properties, antibacterial, antifungal, wound healing, UV filtering, high catalytic and photochemical activity and also has potential advantages in detecting volatile gas [3].

Currently, so much effort has been devoted to study ZnO NPs as a very promising gas sensing due to its high activity, low cost and environmentally friendly feature and semiconductor properties. It is well known that gas sensors is strongly depends on the large surface-to volume ratio it provided that can greatly facilitate gas diffusion and mass transport in sensor material, thus improving sensor performance [4]. On the other hand, the metal oxide nanoparticles have well anti bacterial activities and antimicrobial formulations comprising nanoparticles, which can be used as an effective bactericidal agent [5]. ZnO nanoparticles are synthesized by different methods: direct precipitation, homogeneous precipitation, solvothermal method, sonochemical method, reverse micelles, sol gel method, hydrothermal, thermal decomposition, and microwave irradiation [6].

Recently, researchers have discovered the possibilities of developing nanomaterials using a green approach in an aqueous medium with the help of stabilizing, capping or hydrolytic agents importance due to its simplicity, inexpensive and eco-friendly [7]. Several polysaccharides, including starch, pectin, cellulose, chitin, and chitosan, have found potential uses in the pharmaceutical and biomedical fields [8]. Polysaccharides of chitosan, starch and alginate are particularly interesting as a matrix polymer since their chains possess large numbers of hydroxyl groups that complex well with metal ions and make them a good environment for the growth of metal and semiconductor nanoparticles [9]. Among polysaccharides, the most abundant cellulose and chitosan are not soluble in water and challenging to dissolve in most organic solvents. Alginate has also been shown to be bio and mucoadhesive, biocompatible and nonirritant, thus finding commercial applications which are useful in biomedical applications such as drug delivery, bionanoreactors, nanofiltration, biosensors and antimicrobial activities [10].

Alginate is a readily water-soluble polysaccharide and a desirable candidate for aqueous processing. Alginate was used as a controlled environment for the growth of ZnO NPs [11]. From this point of view, an effort has been made to develop a simple green route to synthesize ZnO nanocubes using alginate in order to achieve controlled synthesis

* Corresponding author.
E-mail address: suganthaaux@gmail.com (V.S. Kumari).

http://dx.doi.org/10.1016/j.sbsr.2016.08.007

of A/ZnO NPs and investigate their structural, optical, thermal, antimicrobial properties and examine the NH_3 sensing performance of such a device at room temperature.

2. 2. Experiments

2.1. Materials

Alginate from brown algae with M_r~48,000–186,000 (Biochemica) Fluka was used in the present study. Zinc acetate and sodium hydroxide were purchased from Merck and used as received. All reagents used were of analytical grade and were used without further purification.

2.2. Fabrication of alginate–nO nanoparticles

Green synthesis of alginate–zinc oxide nanoparticles was successfully fabricated by a simple and cost-effective procedure. In a typical synthetic procedure for the preparation of alginate–ZnO NPs (A/ZnO NPs), 0.2 g Sodium alginate, 1.2 g $Zn(NO_3)_2$.$6H_2O$, and 40 mL distilled water were added into a 100 mL beaker. After full dissolution, 40 mL of 0.125 M NaOH solution was added dropwise under constant stirring. The reaction was allowed to proceed at room temperature for 24 h. Then, the obtained white precipitate was centrifuged at 10,000 rpm for 10 min and collected and washed with deionised water several times to remove the byproducts. After drying in vacuum at 40 °C for 4 h, the final product was obtained as a white powder.

2.3. UV–Visible (UV–Vis) spectroscopy

UV–vis absorption spectra of a water solution of the A/ZnO NPs and a water dispersion of the ZnO micropowder were performed using a commercial Perkin Elmer Lambda 5 spectrophotometer at room temperature with 1 cm optical path length.

2.4. Attenuated total reflectance-Fourier transform infrared (ATR-FTIR) spectroscopy

The chemical structure of the prepared A/ZnO NPs was characterized using an attenuated total reflectance Fourier transform (ATR-FTIR) spectrophotometer (Shimadzu IR affinity —1S). Each spectrum was acquired in transmittance mode on a Quest ATR ZnSe crystal cell by accumulation of 250 scans with a resolution of 4 $cm^{-1}$and a wavenumber range of 4000–400 cm^{-1}.

2.5. Thermo gravimetric analysis (TGA)

Thermo gravimetric analysis of the A/ZnO NPs was carried out using a TGA (Perkin Elmer STA 6000) analyzer. Experiments were carried out under a nitrogen atmosphere and the temperature range 30–800 °C at the heating rate of 10 °C/min in N_2 atmosphere.

2.6. XRD analysis

X-ray diffraction patterns of A/ZnO NPs were recorded with an X-ray diffractometer (XRD; Bruker AXS D8 Advance). The voltage and current used were 40 kV, and a current of 40 mA using Cu K α radiation (k = 0.154178 nm).

2.7. Scanning electron microscope (SEM)

The A/ZnO NPs were mounted on carbon stubs and the images were studied using scanning electron microscope (SEM- JEOL model JJM-6390LV).

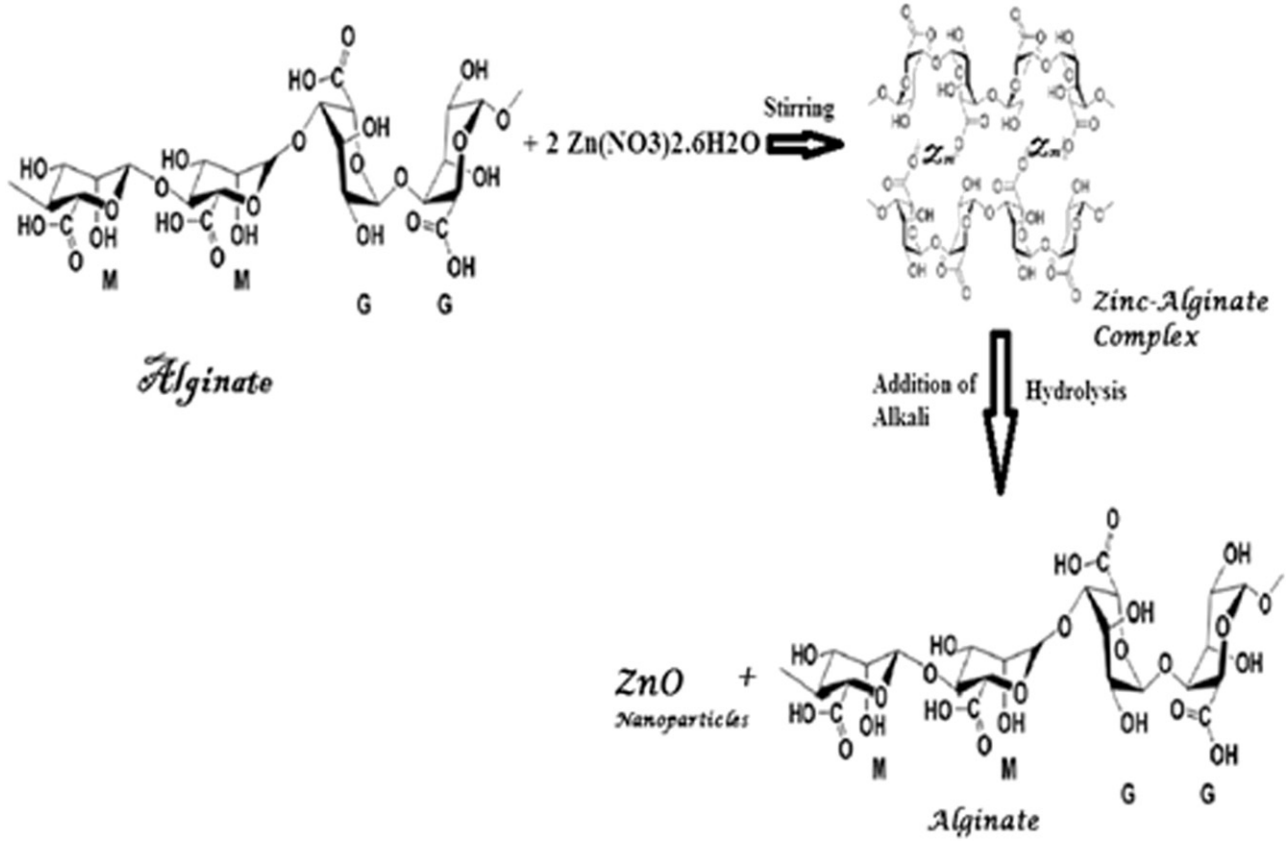

Scheme 1. Possible mechanism of A/ZnO NPs formation.

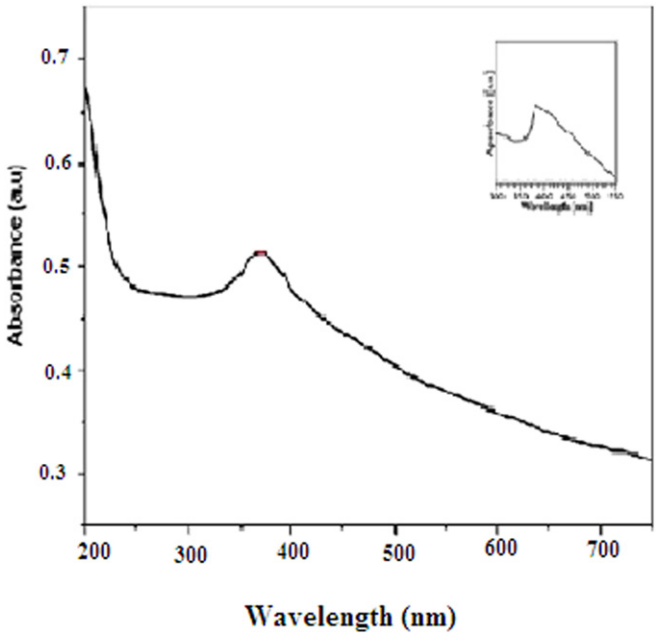

Fig. 1. UV–vis absorption spectra A/ZnO NPs. The inset shows the absorption spectra of the micron size ZnO powder.

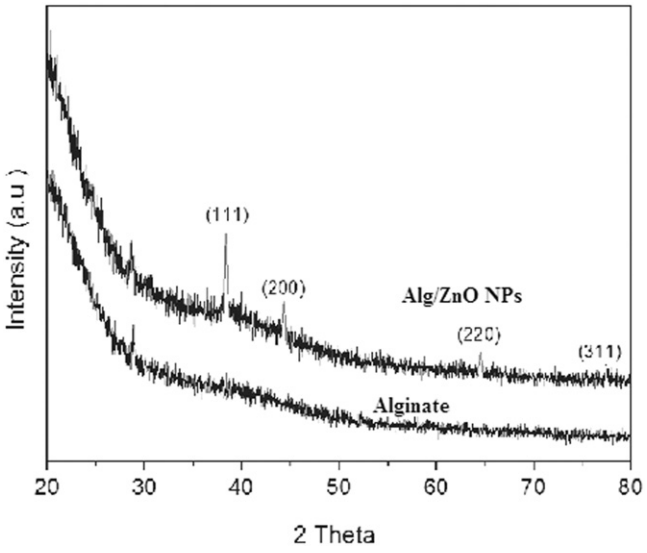

Fig. 3. XRD patterns of alginate and A/ZnO NPs.

2.8. Transmission electron microscopy (TEM)

Transmission electron microscopy measurements were carried out by using a Phillips CM200 instrument with operating voltage 20–200 kV Resolution 2.4A°. The samples were prepared by placing a drop of the A/ZnO NPs water solution onto a carbon coated copper grid.

2.9. Sensing study of ammonia detection

For the sensing study, 25% of ammonia solution is used. Ammonia concentration is varied by diluting ammonia solutions of different concentrations (1 to 100 ppm in deionised distilled water) were prepared right before experiment.

2.10. Antibacterial activity

The antibacterial activity of the were tested pure alginate (G), ZnO micropowder and A/ZnO NPs using well cut diffusion method against *Staphylococcus aureus*, a gram positive bacteria and *E.coli* a gram negative bacteria. Each bacterial isolate was suspended in Mueller Hinton Agar (M-H) for performing antibiotic susceptibility tests and diluted to approximately 10^5 colony forming unit (CFU) per mL. They were flood-inoculated onto the surface of (M-H) agar and then dried. Five-millimeter diameter wells were cut from the agar using a sterile cork-borer and 30 μL of the sample solution were poured into the wells and the plates were incubated for 18 h at 37 °C. Antimicrobial activity was

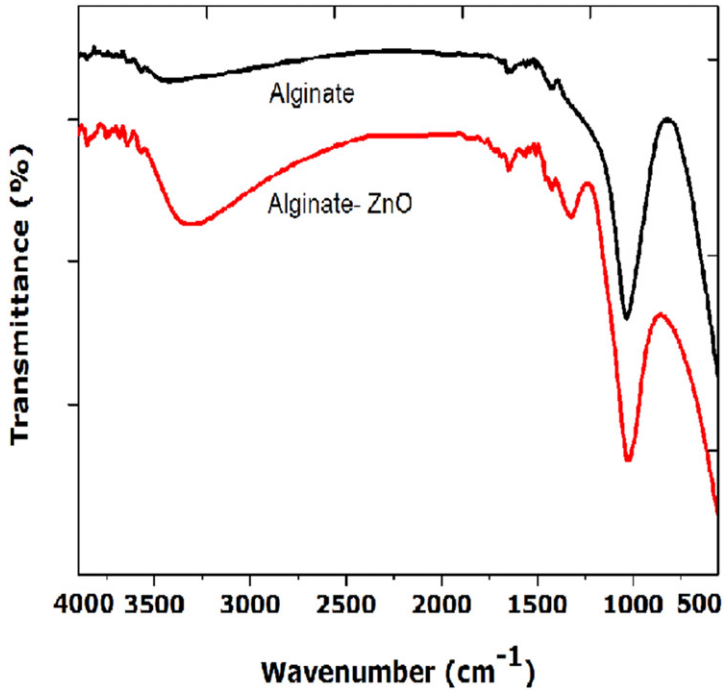

Fig. 2. ATR-FTIR spectra of alginate and the as prepared A/ZnO NPs.

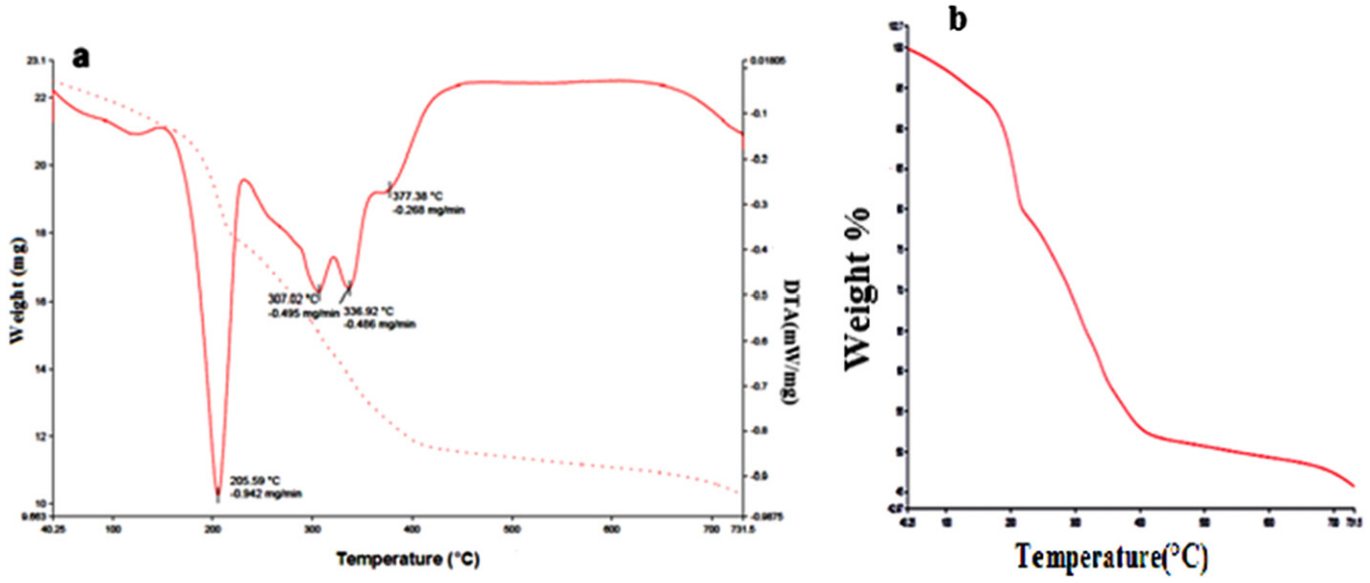

Fig. 4. (a) & (b) TG–DTA curves of the A/ZnO NPs.

evaluated by measuring the diameter of the zone of inhibition in mm against the test microorganisms and the solvent DMSO was used as negative control and ciprofloxacin (positive control) was used as a reference antibacterial agent.

3. Results and discussion

3.1. Mechanism

The formation of the ZnO nanoparticles in the presence of alginate possibly occurs according to following chemical reactions.

$$Zn^{2+} + 4OH^- \rightarrow Zn(OH)_4{}^{2-} \quad (R1)$$

and

$$Zn(OH)_4{}^{2-} \rightarrow ZnO + 2H_2O + 2OH^- \quad (R2)$$

In the first reaction the Zn^{2+} ions react with OH^- creating the precursor $Zn(OH)4^{2-}$, which upon heating bond together forming the cluster $[Zn_xO_y(OH)_z](z + 2y - 2x)^-$. During the ZnO crystal growth, this cluster is incorporated into the lattice. On the other hand, alginate poly G-sequences tend to adopt an ordered confirmation through dimerization in the presence of divalent metals, so they act as a controlled environment for the growth of particles of nanometer sizes.

A plausible mechanism for the formation of A/ZnO NPs has been shown in Scheme.1. It appears that the A/ZnO NPs are encapsulated by the alginate polymeric network structures. The formed alginate polymer networks facilitate the excellent stability of the NPs through electrostatic and steric effects and the hydroxyl groups of the polymeric chains, which further promote the stabilization of A/ZnO NPs. Because of the complexation ability of the polymer with A/ZnO NPs through the hydroxyl groups of the polymeric chains and networks, they surround and protect the particles over longer periods. On the other hand, a strong physical adsorption of the alginate polymer onto the surface of the A/ZnO NPs is also an indication of better stabilization.

3.2. Optical properties

Optical properties of the A/ZnO NPs were evaluated by measuring the absorption spectrum of the nanoparticles using UV–vis spectroscopy. Fig.1. shows the absorption spectra of A/ZnO NPs. In the inset of

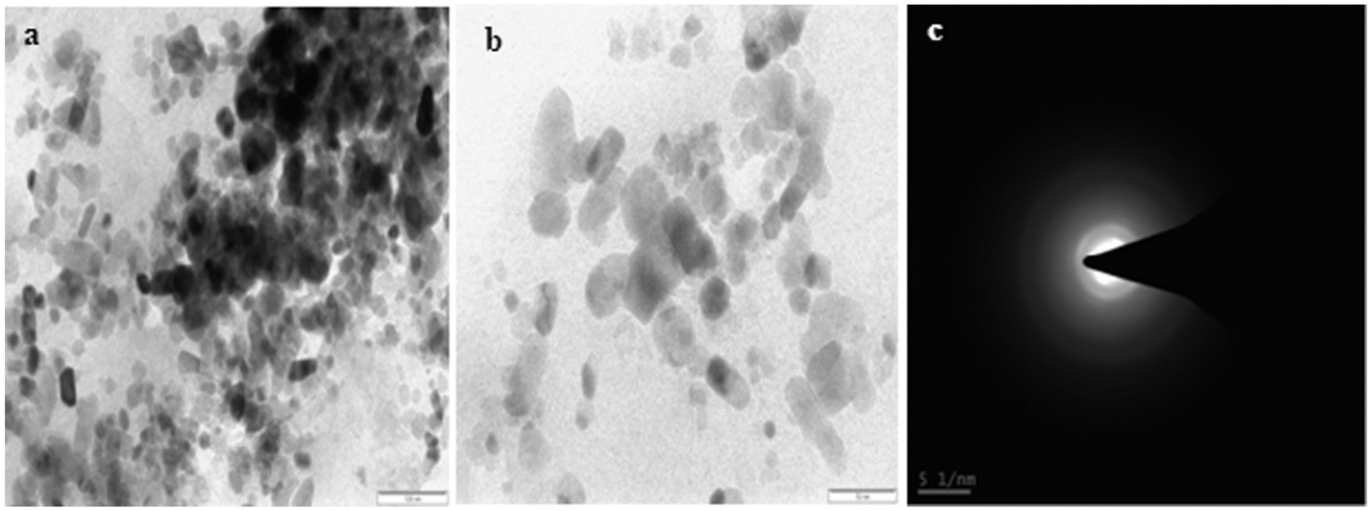

Fig. 5. (a) & (b) TEM of A/ZnO NPs at different magnification (c) Selected area diffraction (SAED) pattern of A/ZnO NPs.

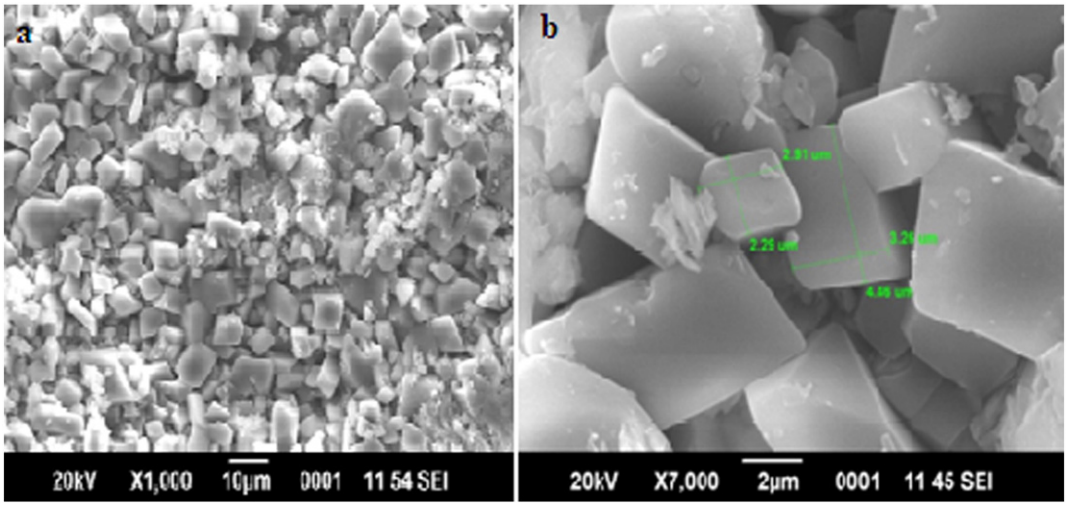

Fig. 6. (a) & (b) SEM micrograph of A/ZnO NPs at different magnification.

the same figure, the UV–vis absorption of the water dispersion of the ZnO micropowder is shown. As can be seen, the positions of the absorption peaks were shifted towards lower wavelength of 369 nm with respect to the absorption of bulk ZnO (380 nm, inset) indicating the presence of nano-size particles. A/ZnO NPs absorbed radiation in the visible regions of 350–400 nm due to the strong surface plasmon resonance (SPR) band transition. Ameen et al. (2013) [12] reported that the appearance of a SPR band in the region 300–400 nm confirmed the formation of ZnO NPs.

3.3. Attenuated total reflectance Fourier transform infrared spectroscopy (ATR-FTIR)

ATR-FTIR spectroscopy was used to assess the polymer chemical groups and the nature of the interactions inside the nanoparticles. FTIR peak assignments of A/ZnO NPs are presented in Fig.2. An absorption peak at about 480 cm^{-1} can be found in the A/ZnO NPs sample; this is a typical IR absorption peak of ZnO, originating from stretching mode of the Zn—O bond [13]. The absorption peaks at 1000 and 1132 cm^{-1} are related to guluronic acid, mannuronic acid, the building blocks of sodium alginate. A peak around 1587 cm^{-1} indicates the presence of carbonyl (CO) group. The absorption peaks at 1400 and 1440 cm^{-1} are related to stretching bands of COO^- groups of alginate. It is found that the intensities of two peaks at 2355 cm^{-1} and 3330 cm^{-1} (induced by CH_2 and OH groups of alginate, respectively) for A/ZnO NPs are obviously weaker than that for alginate. In addition, the bands at about1597and1303cm^{-1}which may be attributed to stretching vibration of COO^- groups in the sugar residues of the polysaccharide molecules, became strong, indicating a successful interaction between the –COOH of sugars and the –OH group on the surface of A/ZnO NPs and formation of COO-Zn [14].

3.4. 3.4 XRD studies

The crystalline natures of the A/ZnO NPs were also confirmed by analysis of the XRD pattern. Fig.3 shows the XRD pattern of the alginate and A/ZnO NPs. It seems that the alginate did not reveal any diffraction peak for ZnO, while the A/ZnO NPs film revealed four distinctive diffraction peaks at 38.5°, 45.6°, 65.3° and 78.6° corresponding to Miller indices (1 1 1), (2 0 0), (2 2 0) and (311) were observed which confirmed the fcc crystalline geometry of A/ZnO NPs based on the above XRD data.

3.5. 3.5 TG–DTA analysis

Fig. 4a &b shows the TG–DTA measurement results of the A/ZnO NPs. The DTA analysis of A/ZnO NPs occurred through three different weight loss steps. The initial weight loss at 50 °C due to loss of residual water. The second major weight loss was observed at, 205 °C which might be due to the thermal decomposition of A/ZnO NPs. The third major weight loss at approximately 377 °C was attributed to the thermo-oxidative decomposition of A/ZnO NPs resulting in various degradation products. The thermal stability of nanocomposite was increased with the formation of A/ZnO NPs.

3.6. Surface morphologies and structural properties

TEM and SEM in Figs.5 and 6 respectively, clearly show the distribution of A/ZnO NPs nanoparticles. The morphology of the A/ZnO NPs was to be cubical and rod and the size range between 20 and 40 nm and from

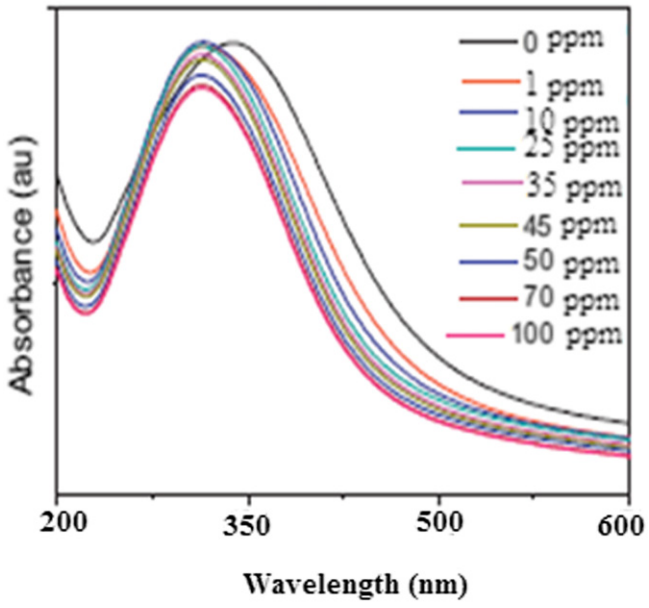

Fig. 7. The plot of changes in spectral absorbance of A/ZnO NPs as a function of various ammonia concentration.

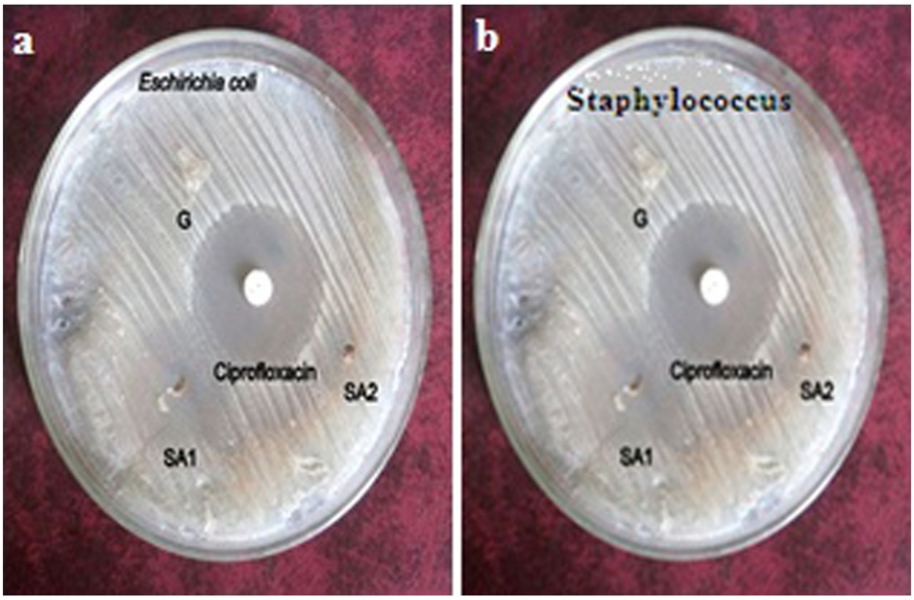

Fig. 8. Antibacterial activity of pure alginate, micron size ZnO powder and A/ZnO NPs. Ciprofloxacin antibiotic (positive control). Abbreviations are 'G' is for pure alginate, 'SA1' is for A/ZnO NPs and 'SA2' is for micron size ZnO powder.

the image it was clearly visible that crystalline presents in the powder material were highly agglomerated. The selected area electron diffraction (SAED) pattern (Fig. 6b) shows distinct bright rings which confirm the preferential orientation of cubical and rod structure. The electronic diffraction pattern (Fig.5) confirmed the formation of the highly crystalline zinc oxide nanostructure with (100), (101) and (110) phases. The formation of A/ZnO NPs with cubic shape is not common, but it has been mentioned in the literature [15].

3.7. Ammonia sensing performance

A/ZnO NPs sensor in various ammonia concentrations at room temperature are shown in Fig. 7. The sensing study of ammonia solution was performed by optical measurement. The absorbance spectra, as a function of ammonia concentration increasing from 0 to 100 ppm. For each measurement, fresh colloidal solutions of A/ZnO NPs are taken. It may be noted that the LSPR peak intensity at 355 nm decreases and another peak appears at 313 nm as the ammonia content is increased. Shifts of LSPR band are usually due to the change in inter-particles distance and the dielectric constant of the surrounding medium. It has been shown that the absorption spectra can be analyzed and the concentration of ammonia can be detected. A new peak at 313 nm appears when ammonia is added to the A/ZnO NPs solution. Because of association of ammonia with NPs lead to the formation of coordination complexes. The sensing property of the NPs solution against increasing ammonia concentration in the range of 1–100 ppm by monitoring the changes in SPR position and amplitude with a UV–Visible spectrophotometer has been reported [16].

3.8. Antibacterial activity

The antibacterial activities of the pure alginate (G), ZnO micropowder and A/ZnO NPs against Gram-positive (*S. aureus*) and Gram-negative (*E. coli*) pathogenic bacteria are shown in Fig.8. As expected, the pure alginate (G) has not shown any antibacterial activity, but the A/ZnO NPs and ZnO micropowder showed antibacterial activity against both Gram-positive and Gram-negative bacteria. ZnO micropowder has lesser antimicrobial activity than green synthesized A/ZnO NPs. Obviously, the antibacterial activity of A/ZnO NPs was varied depending on the microorganisms. It is seen that, ZnO NPs have prominent activities against *E. coli* at 10 mm and are followed by *S. aureus* at 11 mm i.e., they exhibited stronger antibacterial activity against *S. aureus* than *E. coli*. Excellent antimicrobial activities of A/ZnO NPs against *S. aureus* and *E. coli* and the corresponding mechanism of action is A/ZnO NPs may release Zn^{2+} ions, which could penetrate through the cell wall of bacteria and react to the cytoplasmic content and kill bacteria [17].

4. Conclusion

A/ZnO NPs were prepared within an alginate biopolymer by a facile, green and inexpensive technique. The structural properties, morphology, thermal decomposition process, and optical absorption of the nanocomposite were studied. The onset of the absorption of the A/ZnO NPs solutions were shifted towards a lower wavelength due to the nanosize dimensions of the particles. The X-ray diffraction (XRD) analysis showed the crystalline structure, and transmission electron microscopy (TEM) showed the morphology of the A/ZnO NPs to be cubical and rod and the size range between 20 and 40 nm. The endothermic peak with maximum at 377 °C corresponded to the decomposition of the basic zinc nitrate to zinc oxide was confirmed by TG–DTA study. This study also showed that A/ZnO NPs have potent antibacterial activities against *S. aureus* and *E. coli* bacterial cells, than the pure alginate. Further the application of nanoparticles was studied on the aqueous ammonia sensing properties. Colorimetric assays of A/ZnO NPs have shown to be very useful due to their simplicity, high sensitivity, low detection limit of 1 ppm, low cost, fast response time and great reproducibility. This suggests that the present material can be used as a commercial sensor for the detection of ammonia gas.

Acknowledgement

The authors are thankful and grateful to Auxilium College, Management for providing necessary facilities to carry out the present work successfully.

References

[1] A.A. Al-Ghamdi, O.A. Al-Hartomy, M. ElOkr, A.M. Nawar, S. El-Gazzar, F. El-Tantawy, F. Yakuphanoglu, Spectrochim. Acta A 131 (2014) 512–517.
[2] P.C. Nagajyothi, T.N. Minh An, T.V.M. Sreekanth, J. Lee, D.J. Lee, K.D. Lee, Mater. Lett. 108 (2013) 160–163.
[3] F. Namvar, S. Azizi, M.B. Ahmad, K. Shameli, R. Mohamad, M. Mahdavi, P.M. Tahir, Res. Chem. Intermed. 14 (2015) 5723–5730.

[4] P. Rai, S. Raj, K. Ko, K. Park, Y. Yu, Sensors Actuators B Chem. 178 (2013) 107–112.
[5] T.J. Clare-Salzler, Z.J. Zaveri, T.D. Mehta, S. Dolgova, N.V. Chu, et al., Nanosci. Nanotechnol. 12 (2012) 7132–7138.
[6] R.B. Kale, Y.J. Hsu, Y.F. Lin, S.Y. Lu, Superlattice. Microst. 69 (2014) 239–252.
[7] D. Nath, P. Banerjee, Environ. Toxicol. Pharmacol. 36 (2013) 997–1014.
[8] F. Munarin, M.C. Tanzi, P. Petrini, Int. J. Biol. Macromol. 51 (2012) 681–689.
[9] P. Kanmani, J.W. Rhim, Carbohydr. Polym. 106 (2014) 190–199.
[10] K. Varaprasad, G.M. Raghavendra, T. Jayaramuduc, J. Seo, Carbohydr. Polym. 135 (2016) 349–355.
[11] L.V. Trandafilovic´, R.K. Whiffen, S. Dimitrijevic, Brankovic´, M. Stoiljkovic´, A.S. Luyt, V. Djokovic´, Chem. Eng. J. 253 (2014) 341–349.
[12] S.M. Ameen, S. Akhta, H.S. Shin, Orient. J. Chem. 29 (2013) 837–860.
[13] L. Shi, S. Gunasekaran, Res. Lett. 3 (2008) 491–495.
[14] S. Azizi, F. Namvar, R. Mohamad, P.M. Tahir, M. Mahdavi, Mater. Lett. 148 (2015) 106–109.
[15] L. Yu, F. Qu, X. Wu, J. Alloys, Compd. 504 (2010) L1–L4.
[16] S. Peng, J.M. McMahon, G.C. Schatz, S.K. Gray, Y. Sun, Proc. Natl. Acad. Sci. U. S. A. 107 (2010) 14530–14534.
[17] G. Subbiahdoss, S. Sharifi, D.W. Grijpma, S. Laurent, H.C. Van der Mei, M. Mahmoudi, H.J. Busscher, Acta Biomater. 8 (2012) 2047–2055.